Calibration of an Underwater Stereoscopic Vision System

Taufiqur Rahman, James Anderson, Paul Winger
Centre for Sustainable Aquatic Resources (CSAR)
Fisheries and Marine Institute of Memorial University of Newfoundland
St. John's, NL, Canada

Nicholas Krouglicof
Faculty of Engineering & Applied Science
Memorial University of Newfoundland
St. John's, NL, Canada

***Abstract*—Although the problem of terrestrial camera calibration has been studied extensively, this knowledge does not necessarily transfer to the underwater environment directly. Because of the significant differences between the optical properties of the two transfer media, it is necessary to address the task of underwater camera calibration as a unique problem. Correspondingly, this paper studies the differences between terrestrial and underwater camera calibration and shows that the calibrated camera models are significantly different in these two environments. Thus, the necessity for in-situ calibration for an underwater environment is quantitatively ascertained. In addition, an underwater stereoscopic vision system is calibrated employing two calibration algorithms; namely, the Rahman-Krouglicof and the Heikkila algorithm. Since the mathematical formulations of the calibration problem in both environments are identical, a general calibration algorithm can be adopted for an underwater application provided that it is robust enough to overcome the suboptimal imaging conditions of an underwater environment. In order to identify a suitable calibration algorithm for aquatic environments, this paper assesses the stereoscopic performance of the two calibration algorithms in terms of reconstruction error. The experimental data confirms that the Rahman-Krouglicof algorithm is well-equipped to address the peculiarities of underwater 3D reconstruction.**

I. Introduction

In order to obtain a quantifiable representation of an aquatic scene, underwater 3D vision systems exploit the principles of optics in many forms including the geometry and the radiometry of imaging [1], [2], the kinetic relationship of an imaging device and the corresponding target [3], [4], the physics of visible and invisible electromagnetic radiation [5], etc. Besides the conventional systems employing stereoscopic vision (e.g., [1]) or active illumination (e.g., [6], [7]), several sophisticated 3D model acquisition methodologies for underwater scenes have been presented in the literature from recent years; examples include [3]–[5]. From the image sequence acquired by a camera in a known motion, 3D models of stationary underwater objects were constructed in [3]. A monocular system in [4] employs photogrammetric techniques to survey submerged archaeological sites. A relatively small cylindrical sample volume was characterized by an underwater holographic system equipped with a ruby laser in [5]. Despite the elegance of the mathematics and the physics that form the basis of the systems in [3]–[5], stereoscopic vision systems are widely popular because of the simplicity of their construction requiring mostly off-the-shelf components [8].

The imaging geometry of a stereoscopic system is sufficiently defined by the relative position of the lens and the image sensor in each camera, the lens distortion properties of each lens, and the pose of the cameras relative to each other. Utilizing the system's imaging geometry, the position of a 3D point can be triangulated after localizing this point in each of the stereo images (i.e., the stereo-correspondence problem) captured by two cameras. As a result, quantitative understanding of the imaging geometry of a stereoscopic vision system is a prerequisite of stereoscopic reconstruction, which can be derived from the image formation process in each camera. Camera calibration refers to the experimental determination of a set of parameters that computably define this image formation process for a given analytical relationship between the object space and the image space [9]. This analytical relationship (i.e., camera model) is obtained from a pin-hole camera model augmented with a lens distortion model (e.g., [9], [10]). The camera parameters that define the camera model can be categorized into two classes; namely, the intrinsic parameters and the extrinsic parameters. The intrinsic parameters include the internal geometry of the imaging device and the optical distortion properties of the lens. In contrast, the extrinsic parameters define the location and the orientation of the camera in the object space. Subsequently, the stereoscopic imaging geometry is computed from the intrinsic and the extrinsic parameters of each stereo-paired cameras.

Known relative positions of a set of 3D points and their corresponding image positions constitute the point correspondence data, which a conventional camera calibration algorithm (e.g., [9]–[12]) operates on to provide a functionally accurate camera model. Typically, this data is generated by imaging a calibration target that represents a set of 3D points by some feature of the target. For example, centers of a dot pattern and corners of a checker board pattern were used in [10] and [12] respectively. While it is relatively simple to generate point correspondence data in a terrestrial application, underwater imaging is challenging because of the optical phenomena of backscattering and signal attenuation [13] introduced by the transmission medium. Correspondingly, the suboptimal imaging conditions render the task of underwater camera calibration a difficult proposition, which is the focal point of this paper.

This paper is appropriately organized to address all the aforementioned aspects of underwater camera calibration as follows. In Section II, a brief review of the prior art dealing with underwater camera calibration is provided. A mathematical formulation of the camera calibration problem is presented in Section III. In addition, Section IV provides a detailed

978-0-933957-40-4 ©2013 MTS

account of an experimental study that was conducted to understand the differences between terrestrial and underwater camera calibration. An underwater stereoscopic vision system is calibrated in Section V, wherein the quality of the calibrated system model provided by two competing calibration algorithms was assessed in terms of geometric reconstruction. Finally, Section VI offers the concluding remarks.

II. Related Work

Well-established camera calibration techniques in [9]–[12] focus on terrestrial camera calibration; however, prior art dealing specifically with underwater camera calibration includes [14]–[16]. Considering the inherent difficulties associated with calibration of a submerged camera, the aforementioned techniques principally aim to solve the underwater camera calibration problem without requiring a calibration target. For example, the idea of self-calibration (where an image sequence acquired by an underwater camera is employed for calibration exploiting the rigidity constraint of the scene) was adopted in [15] so that a calibration target is not necessary. In addition, [14] and [16] attempt to find an analytical relationship between the terrestrial and the underwater calibration so that the former can be employed to predict the camera parameters in an underwater environment. Nevertheless, reliable calibration data can only be obtained when a submerged calibration target is imaged to establish a number of object space and image space correspondences.

Because the light that forms an image in an underwater camera refracts through multiple media interfaces (e.g., water, lens, air, viewing window of the watertight camera enclosure, etc.), observed lens distortion in the corresponding image is significantly higher than the terrestrial case [4]. Drap *et al.* in [4] theorize that this phenomenon of refraction through multiple media manifests as radial distortion [17] in the image. Since the camera calibration technique in [9] offers robust performance regardless of the degree of lens distortion, it is selected as the preferred camera calibration technique in this paper. However, a standard technique (i.e., [10]) was employed to benchmark the performance of the preferred calibration algorithm. Since a computer implementation of the calibration technique in [10] is readily available, adopting this technique in the benchmarking study was particularly convenient.

III. Formulation of the Camera Calibration Problem

A camera model provides a mathematical relationship between the object space and the image space. This model is conventionally derived from the pin-hole camera model (e.g., [9], [10], [12]) as shown in Fig. 1. Although detailed mathematical account on the pin-hole model can be found in [9], [10], [12], a brief recapitulation is provided here for completeness. In reference to the pin-hole camera model in Fig. 1, the effective focal length f of the camera is the normal distance between the image plane (i.e., sensor) and the optical center of the lens. In addition, the image center (u_0, v_0) is the defined as the point where the optical axis of the lens coincides with the image sensor. It should be noted that the optical axis of the lens is normal to the image plane. A 3D point is defined by the coordinates (x_w, y_w, z_w) with respect to an arbitrarily chosen *world* coordinate frame $\mathrm{X}_w\mathrm{Y}_w\mathrm{Z}_w$. A light

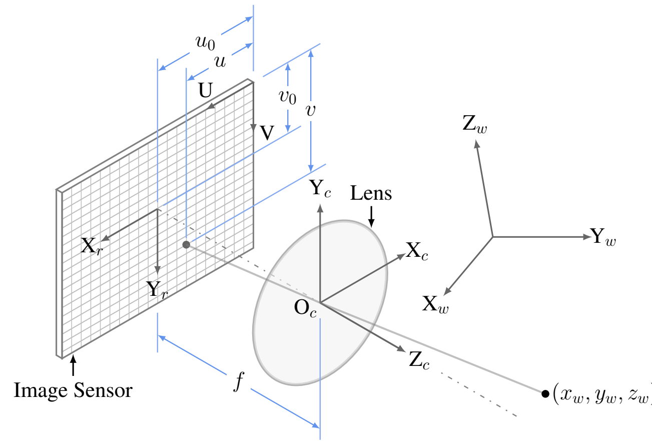

Fig. 1. Pin-hole camera model describing the analytic relationship between an object point (x_w, y_w, z_w) and the corresponding image point (u, v).

ray originating from the 3D point (x_w, y_w, z_w) passes through the optical center O_c of the lens and coincides with the sensor at the image point (u, v), which is defined with respect to the 2D *image* coordinate frame UV. When the image is viewed on a computer screen, the U axis refers to the horizontal axis from left to right and the V axis refers to the vertical axis from top to bottom. The corresponding origin refers to the upper left corner of the computer screen. For convenience of model construction, another coordinate frame $\mathrm{X}_c\mathrm{Y}_c\mathrm{Z}_c$ is introduced, which is termed as the *camera* coordinate frame. The Z_c axis aligns with the optical axis of the lens and the X_c and the Y_c axes are conveniently chosen to be directed in the opposite direction of the U and the V axes respectively. Employing simple geometry, the analytical relationship between the image point and the corresponding object point can be derived in matrix form as shown in (1).

$$\begin{bmatrix} u \\ v \\ 1 \end{bmatrix} = \begin{bmatrix} sf & 0 & u_0 & 0 \\ 0 & f & v_0 & 0 \\ 0 & 0 & 1 & 0 \end{bmatrix} {}^{\boldsymbol{c}}\mathbf{T}_{\boldsymbol{w}} \begin{bmatrix} x_w \\ y_w \\ z_w \\ 1 \end{bmatrix}. \tag{1}$$

In (1), the camera scale factor s accounts for the departure of the sensor pixels from being a square. In addition, the $3{\times}4$ matrix in (1) is called the *camera matrix*. The relative pose of the world coordinate frame with respect to the camera coordinate frame is provided by the $4{\times}4$ homogeneous transformation matrix ${}^{\boldsymbol{c}}\mathbf{T}_{\boldsymbol{w}}$ in (1). As described in [9], ${}^{\boldsymbol{c}}\mathbf{T}_{\boldsymbol{w}}$ can be derived from a unit quaternion $\mathbf{q} = [d\,a\,b\,c]^T$ that provides the relative orientation of the world coordinate frame with respect to the camera coordinate frame, and a position vector $[t_x\,t_y\,t_z]^T$ that localizes the origin of the world coordinate frame with respect to the camera coordinate frame.

The pin-hole camera model does not account for lens distortion, which is a native characteristic of all practical lenses. Correspondingly, in order to obtain a more accurate model of image formation, the pin-hole camera model is augmented with a lens distortion model in (2) that provides a nonlinear relationship between the distorted image point (u_d, v_d) and the undistorted image point (u', v').

$$\begin{bmatrix} u' \\ v' \end{bmatrix} = \begin{bmatrix} u_d \\ v_d \end{bmatrix} + \begin{bmatrix} \bar{u}_d(k_1 r_d^2 + k_2 r_d^4) + \big(2p_1\bar{u}_d\bar{v}_d + p_2(r_d^2 + 2\bar{u}_d^2)\big) \\ \bar{v}_d(k_1 r_d^2 + k_2 r_d^4) + \big(p_1(r_d^2 + 2\bar{v}_d^2) + 2p_2\bar{u}_d\bar{v}_d\big) \end{bmatrix} \tag{2}$$

TABLE I. COMPARISON OF CALIBRATION RESULTS IN TERRESTRIAL AND UNDERWATER ENVIRONMENTS

Parameter	Rahman-Krouglicof		Heikkila	
	Terrestrial	Underwater	Terrestrial	Underwater
s	1.0008	1.0011	1.0008	1.0011
f	8.3133	11.1498	8.3141	11.1344
k_1	+1.0508E-03	-2.5193E-03	+1.0622E-03	-2.5694E-03
k_2	-1.9573E-05	+1.1460E-04	-1.9020E-05	+1.1230E-04
p_1	-1.3235E-04	-5.8442E-04	-1.2705E-04	-5.8635E-04
p_2	+1.6056E-04	+7.8339E-04	+1.4813E-04	+8.1985E-04
u_0	1327.3466	1295.7694	1327.9227	1294.9786
v_0	0931.7374	0954.5705	0931.1679	0955.5021

Here, $\bar{u}_d = u_d - u_0, \quad \bar{v}_d = v_d - v_0, \quad r_d = \sqrt{\bar{u}_d^2 + \bar{v}_d^2}$. In (2), the coefficients of radial and tangential distortion are provided by k_1, k_2 and p_1, p_2 respectively. It should be noted that the distorted image coordinates are viewable in the image output of a camera, while the undistorted image point is a virtual point that assists in formulating a mathematical interpretation of image formation. In an ideal case, the points (u, v) and (u', v') coincide.

In the course of developing the camera model, a total of 14 independent camera parameters have been defined that constitute the camera model. If *unit quaternions* parameterizes the *extrinsic* orientation, 15 parameters are required, of which 14 are independent. In general, the camera calibration problem involves estimating the following parameter vector from point correspondences:

$$\boldsymbol{\theta} = [s\ f\ k_1\ k_2\ p_1\ p_2\ u_0\ v_0\ d\ a\ b\ c\ t_x\ t_y\ t_z]^T .$$

IV. UNDERWATER CAMERA CALIBRATION EXPERIMENT

Point correspondences between the object space and the image space (i.e., world coordinates of an object point and its corresponding image point) constitute the input data for a conventional calibration technique. In order to generate the point correspondences, a calibration target featuring a number of calibration markers is imaged by each stereo-paired camera. Each calibration marker represents an object space point. In a subsequent step, these points are localized in the image space from an image of the target through the application of appropriate image processing algorithms. For an underwater environment, generating the point correspondences can be a challenging task, since the target must also be submerged. As a result, a suitable calibration target must observe several application-specific requirements including superior visibility of the calibration markers representing object space points, water resistance of the structure, provisions for convenient deployment and retrieval, etc. Accordingly, this paper employs a precisely constructed cubic structure featuring dot patterns on two adjacent faces as a calibration target (see Fig. 2). Locations of the dots are known to an accuracy corresponding to the CNC machining precision, which provides an exceptionally accurate set of object space coordinates. A total of 882 calibration markers is featured on the target. These points are equally divided on two planes on a 21×21 square grid with a grid dimension of one inch.

It was claimed in [16] that underwater camera calibration parameters can be inferred from the corresponding in-air parameters, provided the external entry surface (i.e., viewing port) is planar. Specifically, it was shown that the focal length for the camera increases by a factor of 1.333, which is the refraction index of water. In addition, the image center of the camera-lens system is claimed to be identical for the in-air and underwater case. Experimental verification of these hypotheses was conducted in this paper by acquiring 6 sets of point correspondence data for a single camera for each environment. The lens system that is comprised of the viewing port of the watertight enclosure and the imaging lens of the camera was kept identical for both environments. Subsequently, these point correspondence data were calibrated by the Rahman-Krogulicof calibration algorithm in [9] and the Heikkila calibration algorithm in [10]. A set of intrinsic calibration parameters provided by a representative sample from the experimental results is presented in Table I.

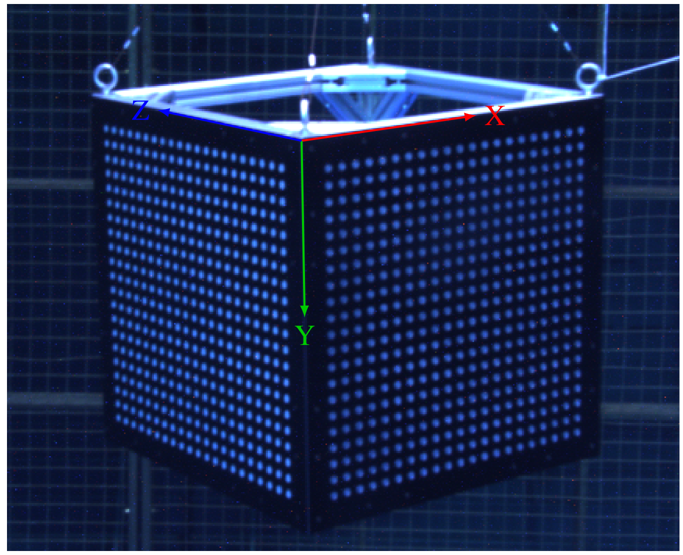

Fig. 2. Calibration target submerged in a flume tank. The positions of all calibration markers are known with respect to an arbitrarily chosen coordinate frame (i.e., world coordinate frame).

TABLE II. CALIBRATED FOCAL LENGTHS IN TERRESTRIAL AND UNDERWATER ENVIRONMENTS

Rahman-Krouglicof			Heikkila		
Terrestrial	Underwater	Ratio	Terrestrial	Underwater	Ratio
8.3133	11.1498	1.3412	8.3141	11.1344	1.3392
8.3192	11.1038	1.3347	8.3197	11.1562	1.3409
8.3143	11.1266	1.3382	8.3167	11.1307	1.3384
8.3208	11.1335	1.3380	8.3248	11.1294	1.3369
8.3128	11.1770	1.3446	8.3125	11.1805	1.3450
8.3085	11.1762	1.3452	8.3083	11.1822	1.3459

TABLE III. CALIBRATED IMAGE CENTERS IN TERRESTRIAL AND UNDERWATER ENVIRONMENTS

#	Rahman-Krouglicof		Heikkila	
	Terrestrial	Underwater	Terrestrial	Underwater
1	(1327.35, 931.74)	(1295.77, 954.57)	(1327.92, 931.17)	(1294.98, 955.50)
2	(1330.21, 906.39)	(1360.38, 852.26)	(1330.14, 906.84)	(1273.52, 981.74)
3	(1334.20, 898.83)	(1358.36, 844.24)	(1333.18, 899.48)	(1361.65, 850.05)
4	(1337.67, 910.02)	(1337.75, 896.84)	(1334.12, 909.25)	(1337.83, 899.42)
5	(1330.78, 913.16)	(1267.22, 979.41)	(1330.86, 913.11)	(1267.82, 981.26)
6	(1332.72, 912.22)	(1269.76, 936.57)	(1332.59, 912.20)	(1271.88, 938.71)

TABLE IV. STATISTICS OF THE ABSOLUTE REPROJECTION ERROR IN PIXELS

Environment	Sample #	Rahman-Krouglicof Mean	Rahman-Krouglicof σ	Heikkila Mean	Heikkila σ
Terrestrial	1	0.2894	0.3530	0.2895	0.3530
	2	0.2434	0.1600	0.2434	0.1600
	3	0.3208	0.4106	0.3205	0.4107
	4	0.2899	0.4451	0.2895	0.4451
	5	0.2380	0.1690	0.2381	0.1690
	6	0.2410	0.1685	0.2411	0.1685
Underwater	1	0.1761	0.0947	0.1764	0.0947
	2	0.1765	0.1058	0.1935	0.1074
	3	0.1797	0.0994	0.1800	0.0993
	4	0.2029	0.1074	0.2030	0.1074
	5	0.2325	0.1386	0.2334	0.1387
	6	0.1769	0.1039	0.1772	0.1037

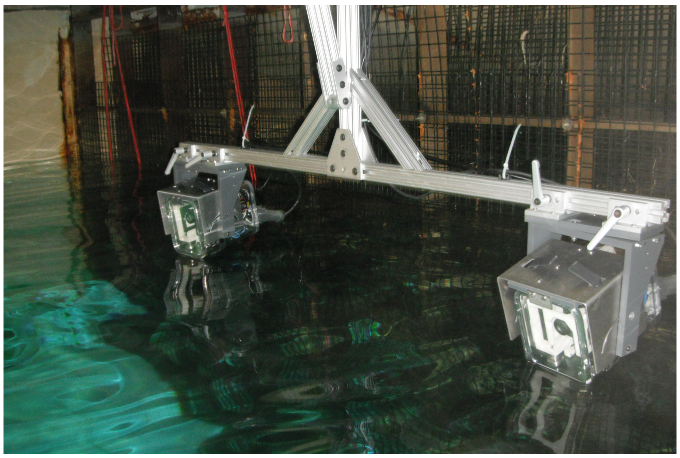

Fig. 3. Underwater stereoscopic vision system being deployed.

A. Data Analysis

The data presented in Table II shows that the ratio of focal lengths obtained for the same camera in a terrestrial and an underwater environment is not exactly 1.333, which is in contradiction with [16]. While this discrepancy can be attributed to measurement error, image noise etc., it must also be realized that these phenomena are a reality for any practical camera calibration. Hence, whether it can be tolerated is a question that must be answered by the accuracy requirements of the respective application. Although a less demanding application may estimate the underwater focal length of the camera from its corresponding terrestrial value, how adversely an inaccurate estimate of the focal length affects underwater measurements should be investigated more closely before the estimation method in [16] can be accepted as a regular practice. In addition, the data presented in Table III confirms that the calibrated image centers in both environments are significantly different. Correspondingly, it must be concluded that an in-situ calibration is required for underwater measurements wherever accuracy is the ultimate goal.

The statistics of the reprojection errors provided by the two calibration algorithms is presented in Table IV. The data exhibits an interesting trend where the reprojection errors for the underwater environment is generally less than those corresponding to the terrestrial case. This is particularly unintuitive, since underwater images are more susceptible to image noise due to the availability of limited ambient light. However, this anomaly can be explained by the fact that the underwater focal length is approximately 33% larger than the corresponding terrestrial value. As a result, the light rays originating from a calibration marker (i.e., a dot on the calibration target) in an underwater environment produce a tighter group on the image plane.

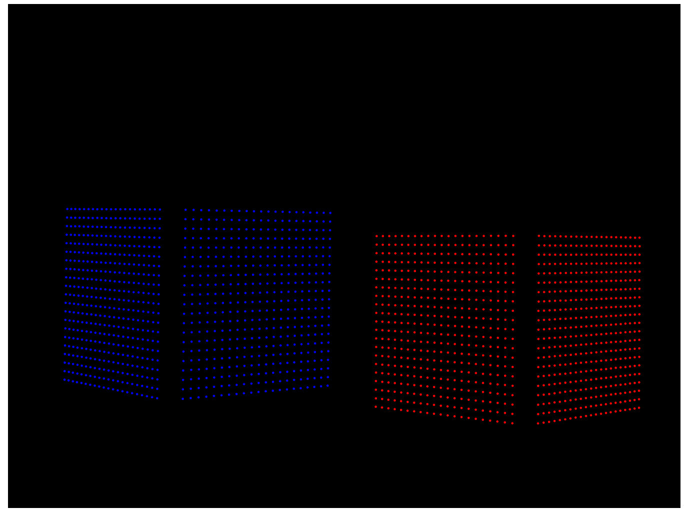

Fig. 4. The calibration target from the point of views of the stereo-paired cameras. The image points of the calibration markers are localized by image processing.

V. STEREO CALIBRATION

The stereoscopic system in this paper features two 5 MP, industrial grade cameras deployed in a flume tank located at Memorial University [18]. Each camera unit is packaged within a watertight enclosure (see Fig. 3). In each of the enclosures, a small form-factor single board computer is coupled with the camera for control and image acquisition. This computer transmits the image stream from the coupled camera to a remote server through a wired Ethernet connection. In addition, the enclosed units are mounted on a trussed structure for convenient deployment and to provide adequate rigidity. After each of the cameras acquires an image of the calibration target, the remote server processes these images to generate the necessary point correspondences for system calibration. Each camera is then calibrated separately employing both calibration algorithms.

In order to assess the quality of the calibration of the stereoscopic system, the calibration target was reconstructed geometrically in this paper. This requires that the stereo triangulation problem [19] be solved. In order to formulate the triangulation problem, (1) can be rewritten as:

$$ {}^{\mathbf{x}}\mathbf{u} = \mathbf{C}_{\mathbf{x}}\,{}^{\mathbf{w}}\mathbf{U}. \tag{3} $$

In (3), ${}^{\mathbf{x}}\mathbf{u} = [u\, v\, 1]^T$ is the image coordinates from $\mathbf{x}$ camera, which can be either the left or the right camera. In addition, ${}^{\mathbf{w}}\mathbf{U} = [x_w\, y_w\, z_w\, 1]^T$ is the coordinates of the object point with respect to the world coordinate frame and $\mathbf{C}_{\mathbf{x}}$ is the generalized camera matrix for the $\mathbf{x}$ camera, which is defined as:

$$ \mathbf{C}_{\mathbf{x}} = \begin{bmatrix} sf & 0 & u_0 & 0 \\ 0 & f & v_0 & 0 \\ 0 & 0 & 1 & 0 \end{bmatrix} {}^{\boldsymbol{c}}\mathbf{T}_{\boldsymbol{w}}. \tag{4} $$

TABLE V. STATISTICS OF THE ABSOLUTE GEOMETRIC DISTANCE BETWEEN OBJECT POINTS & THEIR RECONSTRUCTED COUNTERPARTS

Statistic (mm)	Rahman-Krouglicof	Heikkila
Mean	0.4735	2.8139
Max	3.1686	5.9656
Min	0.0237	0.3823
σ	0.3926	1.3190

For a single object point ${}^{\mathbf{w}}\mathbf{U}$, the image points from the left and the right camera are provided by ${}^{\mathbf{l}}\mathbf{u} = \mathbf{C_l}{}^{\mathbf{w}}\mathbf{U}$ and ${}^{\mathbf{r}}\mathbf{u} = \mathbf{C_r}{}^{\mathbf{w}}\mathbf{U}$ respectively. Given the stereo-paired image points ${}^{\mathbf{l}}\mathbf{u}$ and ${}^{\mathbf{r}}\mathbf{u}$, the triangulation problem attempts to estimate ${}^{\mathbf{w}}\mathbf{U}$ such that

$$\sum_{\mathbf{x}=\{\mathbf{l},\mathbf{r}\}} d({}^{\mathbf{x}}\mathbf{u}, \mathbf{C_x}{}^{\mathbf{w}}\mathbf{U}) \tag{5}$$

is minimum. Here, $d(\cdot,\cdot)$ provides the geometric distance between two points. Although (5) is a trivial problem in the absence of noise, it must be approached as an optimization task for the practical case where a number of noise sources are present. To this end, each camera of the stereoscopic system was calibrated employing the algorithms in [9] and [10]. Subsequently, the generalized camera matrix in (4) was estimated for each calibrated model of the stereo-paired cameras. Finally, the calibration markers were reconstructed by solving the stereo triangulation problem. Several solution methodologies for the triangulation problem can be found in the literature. However, the solution provided in [19] is employed in this paper to reconstruct the calibration cube, since it was proved to outperform the alternative solution approaches [19].

The absolute geometric distance between the known object point coordinates and the reconstructed coordinates (i.e., reconstruction error) is employed as a performance metric to benchmark the quality of the geometric reconstruction. The data presented in Table V clearly shows that the Rahman-Krouglicof algorithm outperforms the the Heikkila algorithm in terms of accuracy in stereo reconstruction of the calibration data. Heikkila advises in [10] that the calibration target should cover the field of view of the camera so that the point correspondence data represent the the image plane uniformly. However, it is difficult to observe this suggestion in practice, since the calibration target must be in the field of view of both cameras simultaneously (see Fig. 4) for stereo calibration. As a result, Heikkila algorithm performs poorly in this case. Moreover, the data in Table V also exhibits the robustness of the Rahman-Krouglicof algorithm, despite the suboptimal nature of calibration data, which originates from a practical implementation issue. The histograms of the reconstruction errors of the 882 calibration markers are presented in Fig. 5.

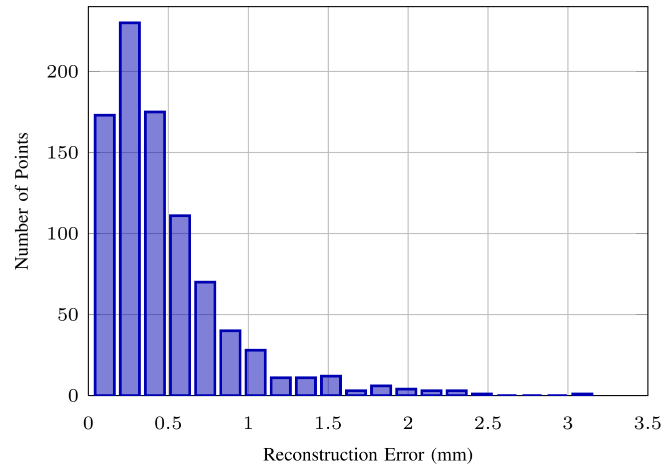

(a) Rahman-Krouglicof

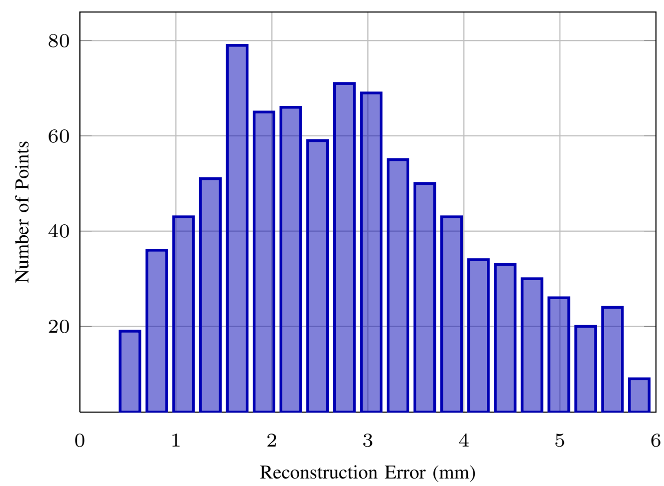

(b) Heikkila

Fig. 5. Histogram of the reconstruction errors obtained by the two calibration algorithms.

VI. CONCLUSION

A calibration procedure for an underwater stereoscopic vision system is presented in this paper. The differences between terrestrial and underwater camera calibration is studied experimentally. The disparity between the calibrated models of the same camera-lens assembly for underwater and terrestrial environments ascertains the need for in-situ calibration for aquatic applications. It was also quantitatively shown that the Rahman-Krouglicof algorithm is robust enough to address the implementation issues that are specifically encountered in underwater stereo calibration.

ACKNOWLEDGMENTS

This paper employs the MATLAB L_∞ toolbox by Dr. Fredrik Kahl for the calculation of reconstruction error. His work is gratefully acknowledged. The authors would like to thank the staff of CSAR, Marine Institute for their help with the acquisition of calibration data. Specifically, Mr. George Legge and Mr. Craig Hollett generously offered their help whenever it was needed. A special thanks is due to Mr. Stephen Reddin for reviewing the paper meticulously that led to several presentational improvements of the paper.

REFERENCES

[1] B. Zheng, H. Zheng, L. Zhao, Y. Gu, L. Sun, and Y. Sun, "Underwater 3d target positioning by inhomogeneous illumination based on binocular stereo vision," in *OCEANS, 2012-Yeosu*. IEEE, 2012, pp. 1–4.

[2] S. Negahdaripour, H. Zhang, and X. Han, "Investigation of photometric stereo method for 3-d shape recovery from underwater imagery," in *OCEANS'02 MTS/IEEE*, vol. 2. IEEE, 2002, pp. 1010–1017.

[3] H. Saito, H. Kawamura, and M. Nakajima, "3d shape measurement of underwater objects using motion stereo," in *Industrial Electronics,*

Control, and Instrumentation, 1995., Proceedings of the 1995 IEEE IECON 21st International Conference on, vol. 2, Nov, pp. 1231–1235.

[4] P. Drap, J. Seinturier, D. Scaradozzi, P. Gambogi, L. Longd, and F. Gauche, "Photogrammetry for virtual exploration of underwater archeological sites," in *XXI CIPA International Symposium*, 2007.

[5] J. Katz, P. Donaghay, J. Zhang, S. King, and K. Russell, "Submersible holocamera for detection of particle characteristics and motions in the ocean," *Deep Sea Research Part I: Oceanographic Research Papers*, vol. 46, no. 8, pp. 1455 – 1481, 1999. [Online]. Available: http://www.sciencedirect.com/science/article/pii/S0967063799000114

[6] S. Tetlow and J. Spours, "Three-dimensional measurement of underwater work sites using structured laser light," *Measurement Science and Technology*, vol. 10, no. 12, p. 1162, 1999.

[7] C. Roman, G. Inglis, and J. Rutter, "Application of structured light imaging for high resolution mapping of underwater archaeological sites," in *IEEE Oceans*, 2010.

[8] F. Bruno, G. Bianco, M. Muzzupappa, S. Barone, and A. Razionale, "Experimentation of structured light and stereo vision for underwater 3d reconstruction," *ISPRS Journal of Photogrammetry and Remote Sensing*, vol. 66, no. 4, pp. 508–518, 2011.

[9] T. Rahman and N. Krouglicof, "An efficient camera calibration technique offering robustness and accuracy over a wide range of lens distortion," *Image Processing, IEEE Transactions on*, vol. 21, no. 2, pp. 626–637, Feb. 2012.

[10] J. Heikkila, "Geometric Camera Calibration Using Circular Control Points," *IEEE Transactions On Pattern Analysis And Machine Intelligence*, vol. 22, no. 10, pp. 1066–1077, 2000.

[11] R. Y. Tsai, "A Versatile Camera Calibration Technique for High-Accuracy 3D Machine Vision Based Metrology Using Off-the-Shelf TV Cameras and Lenses," *IEEE Journal of Robotics and Automation*, vol. 3, no. 4, pp. 323–344, 1987.

[12] Z. Zhang, "A Flexible New Technique for Camera Calibration," *IEEE Transactions On Pattern Analysis And Machine Intelligence*, vol. 22, no. 11, pp. 1330– 1334, 2000.

[13] J. S. Jaffe, K. D. Moore, J. McLean, and M. Strand, "Underwater optical imaging: status and prospects," *Oceanography*, vol. 14, no. 3, pp. 66–76, 2001.

[14] J. Lavest, G. Rives, and J. Lapresté, "Underwater camera calibration," *Computer Vision ECCV*, pp. 654–668, 2000.

[15] N. Gracias and J. Santos-Victor, "Underwater video mosaics as visual navigation maps," *Computer Vision and Image Understanding*, vol. 79, no. 1, pp. 66–91, 2000.

[16] J. Lavest, G. Rives, and J. Lapreste, "Dry camera calibration for underwater applications," *Machine Vision and Applications*, vol. 13, no. 5, pp. 245–253, 2003.

[17] D. C. Brown, "Close-Range Camera Calibration," *Photogrammetric Engineering & Remote Sensing*, vol. 37, no. 8, pp. 855–866, 1971.

[18] P. D. Winger, H. DeLouche, and G. Legge, "Designing and testing new fishing gears: the value of a flume tank," *Marine Technology Society Journal*, vol. 40, no. 3, pp. 44–49, 2006.

[19] F. Kahl and R. Hartley, "Multiple-view geometry under the L_∞-norm," *Pattern Analysis and Machine Intelligence, IEEE Transactions on*, vol. 30, no. 9, pp. 1603–1617, 2008.